



Speciation and dipole re-orientation dynamics of glass-forming liquid electrolytes: Li[N(SO₂CF₃)₂] mixtures of 1,3-propanesultone or tetrahydrothiophene-1,1-dioxide.

Journal:	<i>Faraday Discussions</i>
Manuscript ID	FD-ART-03-2024-000050.R1
Article Type:	Paper
Date Submitted by the Author:	17-Apr-2024
Complete List of Authors:	Umebayashi, Yasuhiro; Niigata University, Graduate School of Science and Technology Otani, Erika; Niigata University, Graduate School of Science and Technology Watanabe, Hikari; Tokyo University of Science - Noda Campus, Department of Pure and Applied Chemistry; Tokyo university of Science Han, Jihae; Niigata University, Graduate School of Science and Technology

Speciation and dipole re-orientation dynamics of *glass-forming liquid electrolytes*: Li[N(SO₂CF₃)₂] mixtures of 1,3-propanesultone or tetrahydrothiophene-1,1-dioxide.

Yasuhiro Umebayashi^{1,*}, Erika Otani¹, Hikari Watanabe², Jihae Han¹

¹ Graduate School of Science and Technology, Niigata University, 8050 Ikarashi, 2-no-cho, Nishi-ku, Niigata, 950-2181, Japan; E-mail: yumescc@chem.sc.niigata-u.ac.jp

² Department of Pure and Applied Chemistry, Faculty of Science and Technology, Tokyo University of Science, 2641 Yamazaki, Noda, Chiba 278-8510, Japan

† Electronic supplementary information (ESI) available. See DOI:

Abstract

Recently new ionic fluids such as super-concentrated electrolyte solutions, solvate ionic liquids and deep eutectic solvents attracted much attention in the field of the liquid electrolytes for the next generation electrochemical devices and processes. Basic composition of these new ionic fluids is similar among them; solvent and a large/excess amount of salt mixtures, though the solvent is sometime solid at ambient temperature. Here, we found and demonstrated that LiTFSA (TFSA = $(\text{CF}_3\text{SO}_2)_2\text{N}^-$) mixtures with 1,3-propanesultone (PS) or tetrahydrothiophene-1,1-dioxide (SL) yield a homogeneous liquid at room temperature at wide range of composition. In order to clarify unique high Li^+ transference number in these mixtures, speciation and dipole reorientation dynamics were studied for these mixtures to be evident large scale size aggregates formation in these mixtures.

Introduction

To achieve sustainable society, it is crucial to realize next generation electrochemical devices and/or processes such as secondary batteries of higher energy density and electrodeposition of higher efficiency. Room-temperature ionic liquids had been attracted much attention as new class of electrolytes during last a few decades. Further new electrolytes are currently focused such as super-concentrated solutions [1, 2], solvate ionic liquids [3-6] and deep eutectic solvents [7] *via* room-temperature ionic liquids. These new electrolytes are frequently consisted of similar components; solvent and a large/excess amount of salt mixtures. As Angell mentioned, the first member of this class electrolyte would be hydrate melts like $\text{CaNO}_3 \cdot 4\text{H}_2\text{O}$. [8-10] It is easily speculated the salt lattice energy should be reduced by containing small amounts of solvent molecules to lower the melting point. However, physicochemical or thermodynamic definition is still unclear for these electrolytes. Recently, we attempted to clarify the definition and propose less than 1 % relative solvent activity to its neat liquid. [11]

From both the scientific and industrial viewpoints, one of the most important properties of liquid electrolytes is ionic transport one as conductivity and viscosity. As Angell proposed, Walden rule or product is useful because this empirical rule generally well hold in the wide range of liquid electrolytes. [12] In this sense, rotational motion of ions and solvents in solution are significant, as well established as the Stokes-Einstein-Debye (SED) equation. [13] Fig. 1 shows viscosity vs. relaxation time plots for 43 polar organic solvents that observed as the dipole re-orientation by means of the dielectric relaxation spectroscopy (DRS). According to the SED relationship, viscosity should be proportional to the relaxation time. The slope is unity for the solid line shown in the figure,

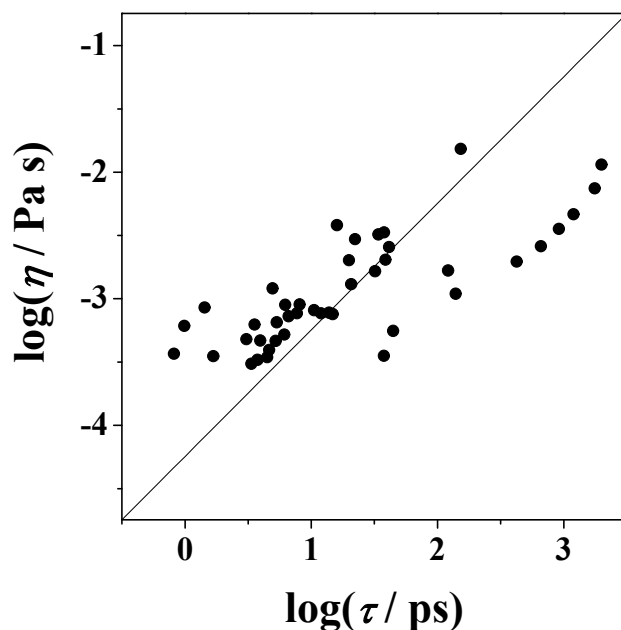


Fig. 1 Relationship between viscosity and relaxation time determined with the DRS for 43 organic solvents.

which clearly exhibits the SED relationships generally holds among a large number of polar solvents. On the other hand, we found super-ionic proton conduction in *pseudo* protic ionic liquids and demonstrated that the acetate/acetic acid rotational motion plays crucial role in this super-ionic proton conduction with the DRS technique. [14] Similarly, we recently found quite slow relaxations exist in the glyme type solvate ionic liquids, and pointed out that this quite slow relaxation could be closely related with specific lithium ion conduction that contains combination of the solvent/anion exchange of lithium ion and their rotational motion. [15]

In this contribution, we mainly discuss two subjects; 1) *glass-forming liquid electrolytes* as a new class of liquids and 2) their speciation and dipole re-orientation dynamics. 1,3-propanesultone (propane sultone: PS) is a 5 membered ring sulfonic acid ester and analogues of tetrahydrothiophene-1,1-dioxide (sulfolane: SL). As easily expected by their molecular structures and electrostatic potentials shown in Fig. 2 and Table 1, the solvating ability to the lithium ion of PS should be weaker than that of the SL. Dokko *et al.* found that Li^+ diffuse fastest than the anion and the SL in super-concentrated lithium salt SL solutions. [16, 17] This unique behavior is similar for the lithium salt PS solutions as shown in Fig. S1 in the supporting information.

Table 1 Atomic partial charge of the sulfonyl oxygen atoms, bond lengths, atom-atom distances and dipole moments with the ChelpG method at the HF/6-31G(d)//MP2/cc-pVTZ levels of theories for PS and SL.

	PS	SL
Charge (O)	-0.48	-0.52
S-O / Å	1.47	1.49
O...O / Å	2.57	2.59
Dipole Moment / Debye	5.59	4.98

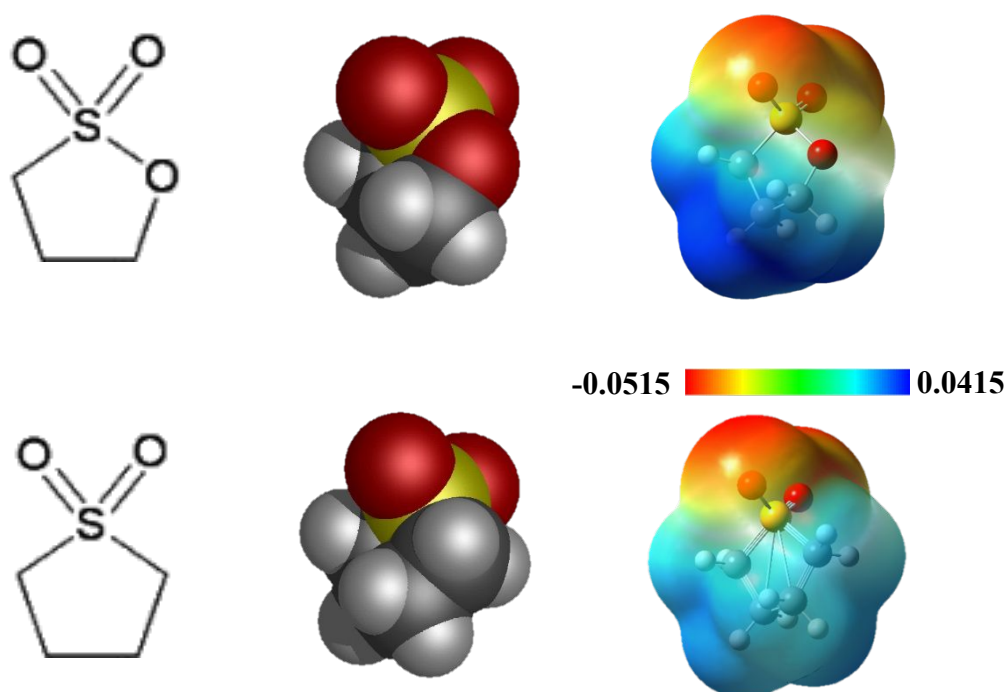


Fig. 2 Molecular structures of 1,3-Propanesultone (PS: upper panels) and tetrahydrothiophene-1,1-dioxide (SL: lower panels), their CPK models and the electrostatic potential with the ChelpG method at the HF/6-31(d)//MP2/cc-pVTZ levels of theories.

Glass-forming liquid electrolytes

Before detailed discussion, it is worth mentioning the concept of recent new ionic fluids such as super-concentrated solutions, solvate ionic liquids and deep eutectic solvents. As aforementioned, the concepts of these ionic fluid are currently similar; i.e., those consist of solvent and a large or excess amount of salt. With regard to ionic liquids, though there are some representations [18-21], their definition is currently clear. Angell suggested

that ionic liquids be defined as liquids composed solely of ions, in principle, with melting points below 100°C, and also classified the ionic liquids into four categories. [22] As aforementioned, we recently proposed that salt and solvent mixtures that have less than 1 % component solvent activity relative to that of the neat solvent could be practically identical to the ionic liquids. [11] In addition, the definition is also unclear for the super-concentrated electrolyte solutions such as the Water-in-salt. It is unclear whether the super-concentrated electrolyte solutions are the same as or different from concentrated solutions as an extension of conventional dilute solutions.

On the other hand, the eutectic mixtures should be absolutely different solutions compared to the ionic liquids, solvate ionic liquid and super-concentrated electrolyte solutions. The term of eutectic has been used by Guthrie in 1884 for the first time [23]. However, it should be clear that a eutectic mixture is a homogeneous mixture that has a melting point lower than those of the constituents and that the lowest melting point over all the mixing ratios and the composition are called the eutectic temperature and the eutectic composition. As far as we are aware, deep eutectic solvents were used for choline chloride and urea mixtures for the first time [7]. Abbott et al. noted a behavior of deep melting point depression in eutectic compositions of choline chloride and urea and called them deep eutectic solvents. In fact, according to the phase diagram, the eutectic composition should be choline chloride : urea = 1 : 2. However, the physicochemical or thermodynamic definitions for the deep eutectic solvents are still unknown. Among them, some do not seem to indicate eutectic points at the eutectic composition. AlCl₃-amide and AlCl₃-carbamide systems also yield molten salt mixtures at ambient temperature. It was considered that AlCl₃ dissolves in the solvents and disproportionation reactions; $2\text{AlCl}_3 \leftrightarrow \text{AlCl}_2^+ + \text{AlCl}_4^-$ occurs, so that these mixtures were first proposed as ionic liquids composed of an aluminum dichloro complex cation $[\text{AlCl}_2(\text{solvent})_n]^+$ instead of an organic cation and a tetrachloroaluminate anion $[\text{AlCl}_4]^-$. [24] After that, AlCl₃-amide and AlCl₃-carbamide systems are thought as eutectic mixers or deep eutectic solvents, [24-27] though, no phase diagram is reported for them as far as we know. On a phase diagram, the eutectic temperature is seen as the eutectic point. For this kind of mixtures, the eutectic composition should be specific and fixed based on the Gibbs' phase rule. In this meaning, it can be said that choline chloride and urea mixture is a typical eutectic mixture. Here, let us go back to the Wilkes' chloroaluminate ionic liquids. [28, 29] In the phase diagram of AlCl₃-1-ethyl-3-methylimidazolium chloride (C₂mimCl) and AlCl₃-1-ethylpyridinium chloride mixtures, specific and fixed eutectic points can be recognized at a glance. [30] Furthermore, these melting points at the eutectic compositions extremely low relative to other non-eutectic composition and yield narrow deep valley.

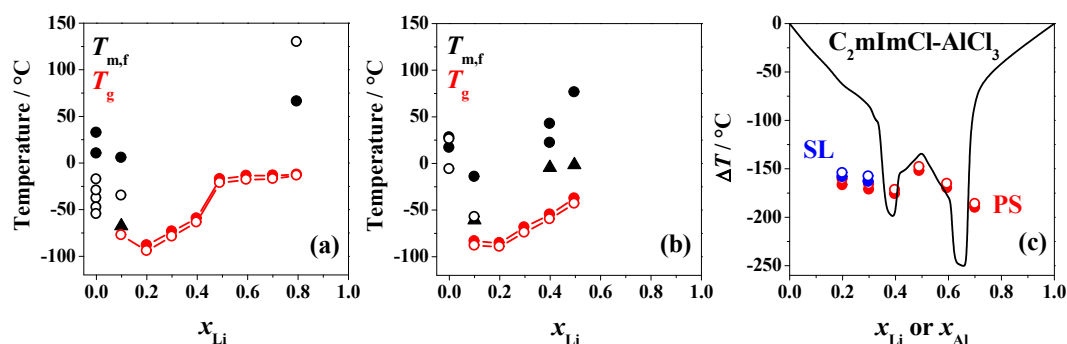


Fig. 3 Composition dependence of thermal anomalies in binary mixtures of LiTFSA-PS (a) and LiTFSA-SL (b). The temperature decline from the heating and cooling processes are shown in closed and open symbols, respectively. The black, red circles and the triangle indicate the melting/freezing points (T_m/T_f), the glass transition point (T_g) and the temperature at which the hot crystallization occurs. (c) The temperature lowering (ΔT) from the ideal melting/freezing point to the observed melting/freezing/glass transition point for the LiTFSA-solvent mixture. ΔT of the $C_2mimCl-AlCl_3$ mixture is shown as a solid line for comparison. x_{Al} represents the mole fraction of $AlCl_3$ salt.

Based on the above discussion, we again recognize importance of the phase diagram for the solvent mixtures with a large and/or excess amount of salt. Fig. 3a and 3b shows roughly drawn phase diagrams for LiTFSA (TFSA: $N(SO_2CF_3)_2^-$)-PS and LiTFSA-SL systems. Differential scanning calorimetry (DSC) and Thermogravimetry (TG) thermograms TG are also shown in Fig. S2 and S3, respectively. As clearly shown in the DSC thermograms for neat PS and SL, these solvents have solid/solid phase transition probably due to the plastic crystal phase. For both systems, with adding LiTFSA salt, the peak arising from melting/freezing disappeared, followed by that ascribable to the solid/solid phase also transition getting lost. The thermal anomalies only found for the glass transition in the range of $0.1 < x_{Li} < 0.8$ for PS and $0.1 < x_{Li} < 0.4$ for SL, where x_{Li} stands for the mole fraction of LiTFSA with T_g (glass transition temperature) increasing up to around $-13\text{ }^\circ\text{C}$ for PS and $-38\text{ }^\circ\text{C}$ for SL as the increase of the LiTFSA. It should be noted that hot crystallization was observed at $x_{Li} = 0.1$ for both systems, though both molecules of small molecular weight. These facts suggest that both of mixtures of a specific composition range behave like a polymer or a gel, hence it could be said that these mixtures of the respective specific composition range should be a new class of liquids called *glass-forming liquid electrolyte*, not super-concentrated solutions, solvate ionic liquids and deep eutectic solvents. One of the most important features of the glass-forming liquid electrolyte is the melting/freezing temperature lowering down to around

the room temperature. One of the most important characteristics of the *glass-forming liquid electrolytes* is that their melting/freezing temperatures drop to near room temperature. The temperature lowering, $\Delta T = T_{\text{ideal}} - T_{\text{m/f/g}}$ is shown in Fig. 3c, where T_{ideal} and $T_{\text{m/f/g}}$ represent the ideal melting/freezing point and the observed melting/freezing/glass transition point for the mixture. T_{ideal} should be given as $T_{\text{ideal}} = T_{\text{m/f, 1}} + x_2 (T_{\text{m/f, 2}} - T_{\text{m/f, 1}})$ where $T_{\text{m/f, 1}}$, $T_{\text{m/f, 2}}$ and x_2 stand for the melting/freezing point for component 1 or 2, and the molar fraction of the component 2, respectively. ΔT of $\text{C}_2\text{mimCl-AlCl}_3$ mixtures also shown in Fig. 3c for comparison. The ΔT of both mixtures is about 150°C , comparable to that of the $\text{C}_2\text{mimCl-AlCl}_3$ mixture. [30] Here, it should be emphasized that the main motivation in this work is to clarify currently vague electrolyte solutions containing solvent and a large or excess amount of salt. As is well known, a numerous number of ionic liquids, super-concentrated electrolyte solutions exhibit the glass transition. We consider that the glass-forming liquid electrolytes should contain a part of ionic liquids and the super-concentrated electrolyte solutions, yet it absolutely differs from (deep) eutectic solvents.

Speciation and dipole re-orientation dynamics

High ionic conductivity or high transference number of Li^+ in solutions plays a key role for realization of high-energy density rechargeable batteries. Such ion transport properties in solutions are governed by the inter-molecular potentials. Structural knowledge of solutions, which is silhouette of the inter-molecular potentials, can be obtained as radial distribution functions or pair correlation functions by X-ray/neutron scattering techniques or molecular dynamics, Monte Carlo simulations. On the other hand, Raman/IR spectra as a vibrational spectroscopy frequently used for electrolyte solutions consisted of the anion/solvent of polyatomic molecules. Formation distribution functions determined by analyzing Raman/IR spectra can give mean solvation number or mean anion binding number, which is just stoichiometric number of the ionic species existing in solutions. For this purpose, the MCR-ALS (multi curve fitting-alternative least squares) technique [31, 32] seems to be useful. We recently developed the CLSA (complementally least squares analysis) technique [11] that similarly gives the formation distribution functions of the anion/solvent in solutions.

The CLSA was applied to LiTFSA-PS and LiTFSA-SL systems to evaluate mean solvation numbers or mean anion binding numbers to the Li^+ for LiFSA-PS as shown in Fig. 4. As clearly exhibited in this figure, mean two solvent molecules and one anion directly coordinated Li^+ aggregated species of $[\text{Li}(\text{solvent})_2(\text{TFSA})]$ as a constituent unit mainly exist in both mixtures at a larger LiTFSA concentration of 3 mol dm^{-3} . As

expected,

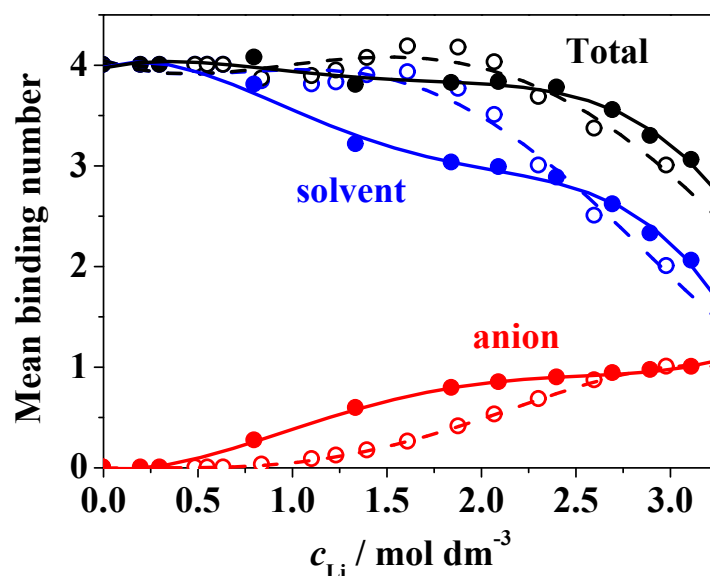


Fig. 4 Mean solvation numbers (MSN) and mean anion binding numbers (MABN) for LiTFSA-PS (closed) and LiTFSA-SL systems (open), respectively, evaluated with the CLSA. Total is shown in black, which is the sum of MSN and MABN. MSN and MABN are shown in blue and red, respectively.

from the weaker solvation ability of PS relative to SL, the contact ion-pair (CIP) and/or the aggregates (AGG) formations occur at a lower LiTFSA concentration in PS than SL. Raman scattering factors and formation distribution functions are also shown in Fig. S5 and S6. For both mixture systems, the respective solvent and anion exist as 3 species; free, bound1 and bound2 for the solvent and free, CIP/AGG and AGG for the anion. Free can be ascribed to the solvents in bulk and those in the Li^+ solvation shell higher than the second one for the solvents, and free anion and those in the Li^+ coordination shell higher than the first one for the anion. Solvent bound1 can be assigned to directly coordinated solvent molecules in the solvated Li^+ and in the CIP and/or the AGG and anion CIP/AGG also to the latter. Solvent bound2 and anion AGG can be attributed to the bridging ones in the Li^+ -TFSA-solvent aggregates. DFT calculation performed for some typical models for the CIP and AGG at the B3LYP/cc-pVDZ level of theory to obtain the optimized geometries and theoretical Raman spectra as shown in Fig. S7-S10. A Raman scattering factor for the CIP/AGG is larger than those for free, which suggests that the CIP/AGG contains a few anions. Similarly, a Raman scattering factor for the AGG is the most intense, which indicates that the AGG should include several anions. It is considered that the AGG formation in highly concentrated lithium salt plays key role for the largest

self-diffusion coefficient for the Li⁺ in the super-concentrated lithium salt SL solutions. [17] Here, the AGG formation is directly evidenced in LiTFSA-PS and LiTFSA-SL mixture systems.

Knowledge on the rotational motion in solutions can be obtained some experimental techniques. By means of the DRS, the dipole reorientation relaxation in a liquid can be observed as a complex primitivity $\varepsilon^* = \varepsilon' + i\varepsilon''$, where ε' , ε'' and i represent a relative dielectric constant, a dielectric loss and an imaginary unit, respectively. DRS has some advantages against NMR; 1) DRS can determine both of the relaxation time and strength for the respective dipole of polar species in solutions, while NMR gives only a time-averaged relaxation time due to the chemical exchange and 2) the relaxation strength is related with an effective dipole moment of the polar species in solutions, so that a space scale for the dipole can be obtained in some case. On the other hand, DRS has also a weak point; it is difficult to the deconvolute and assign the observed relaxation when some relaxation times are close among them. In addition, it may be hard to observe the dipole reorientation relaxation of a short lifetime polar species such as the solvent separated and solvent shared ion-pairs. DRS is now used as new technique for speciation analysis and/or dipole re-orientation dynamics of Li and Mg salt solutions [33-39]. Among them, the attribution of SIP and CIP is not always correct, considering the lifetime of the labile/inert ion-pairs.

The observed complex permittivities and typical deconvolution results using superposition of the Debye relaxation model for both systems are shown in Fig. S11. The fastest relaxation composed of two Debye functions can be ascribed to the bulk solvent molecules. However, the assignment is difficult for two of newly appeared relaxation upon addition of LiTFSA. Here, we attempted to entirely different approach from the conventional DRS analysis. The relaxation strength for i th polar species, S_i , can be expressed as the Cavell equation [40, 41];

$$S_i^* = S_i \frac{2\varepsilon_s + 1}{\varepsilon_s} \frac{k_B T \varepsilon_0}{N_A} = \mu_{i, eff}^2 c_i$$

, where ε_s , ε_0 , k_B , N_A and μ_{eff} T are the relative permittivity, permittivity in vacuo, the Boltzmann constant, the Avogadro number, the absolute temperature and the effective dipole moment, respectively. The effective dipole moment represents that in solution, not gas phase, so that it would be more useful to discuss polar species in solution. Discussions are given later in detail on the evaluation of the effective dipole moment based on the Cavell equation. On the other hand, the Cavell equation tells us for the relaxation strength, in other words, the intensity in DRS to be directly proportional to the polar species concentration, as well as Raman spectra. This suggests the DRS intensity, particularly

that in the imaginary part should be directly correlates with the Raman intensity. Consequently,

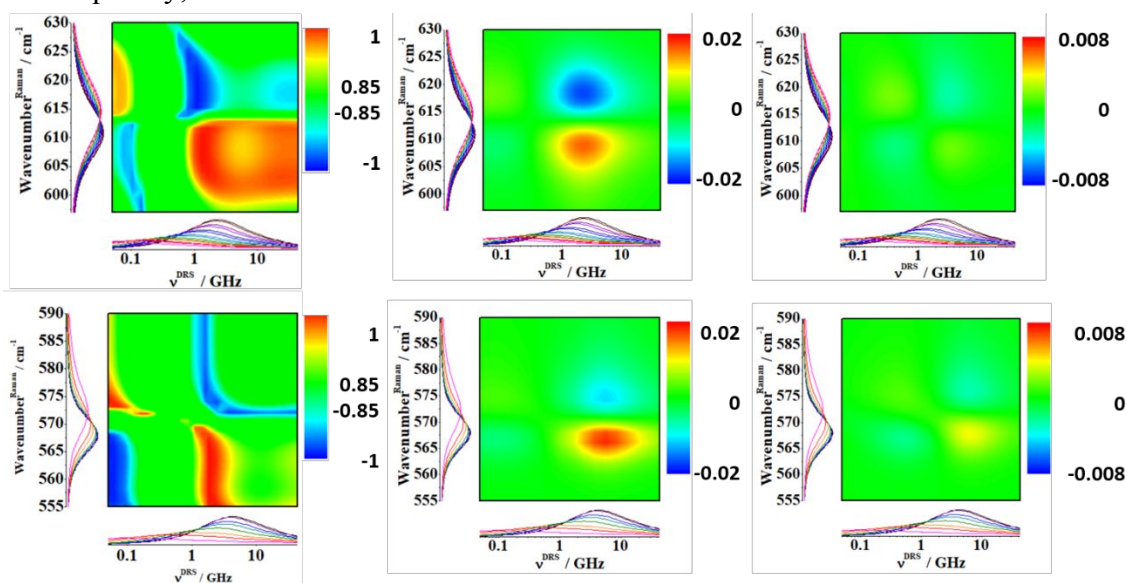


Fig. 5 2D correlation analysis between the Raman spectra of solvents and the dielectric loss (imaginary part of the complex permittivity). Left panels show the Pearson's correlation coefficients, middle and right panels display synchronous, and asynchronous of the Noda-Ozaki 2D hetero-correlation spectroscopy, respectively. Noda-Ozaki 2D hetero-correlation spectroscopy is normalized with the maximum absolute value among the synchronous correlation. Red and blue represent high positive and negative correlation, respectively. Green corresponds to within the value of 0.85 in the Pearson's correlation coefficients and around 0 in the Noda-Ozaki 2D hetero-correlation spectroscopy. The color mapping for asynchronous is expanded by a factor of 2.5 due to the weak correlation. The upper and lower panels are those for LiTfSA-PS and LiTfSA-SL systems, respectively.

as the first step, the MCR-ALS analysis was applied to the DRS data as exhibited in Fig. S12. For both systems, the relaxations of the three species were necessary to describe the observed dielectric loss spectra based on the eigenvalues. The observed dielectric spectra were reproduced with the Hamilton R factor of 2.2 and 2.3 % for the PS and SL system, respectively. This is quite suggestive to ascribe the observed relaxation to the chemical species in solutions. However, thus evaluated resolved relaxations and resolved concentration seem to lose physical meaning; the resolved relaxations for the species2 and species3 cannot be described by using a sole model function such as Debye, Cole-Cole and Cole Davidson.

As the second step, we applied two types of Raman/DRS two-dimensional (2D) correlation analysis to both mixtures. Here, 2D means the apparent Raman spectra, which is the Raman spectra divided by the scattering species concentrations, and the dielectric loss (the imaginary part of the complex permittivity). The first one is simple Pearson's correlation coefficient [42] and the second one is the Noda-Ozaki 2D hetero-correlation spectroscopy [43, 44], as shown in Fig. 5 and 6 for PS and SL systems, respectively. Pearson's correlation coefficient is defined as the ratio between the covariance of two variables and the product of their standard deviations. Details of the Noda-Ozaki 2D hetero-correlation spectroscopy is described in supporting information. One of the characteristics of the Noda-Ozaki 2D hetero-correlation spectroscopy is to express the correlation between two different spectra in terms of two kinds of correlations called synchronous and asynchronous. Synchronous correlation is the relationship between two

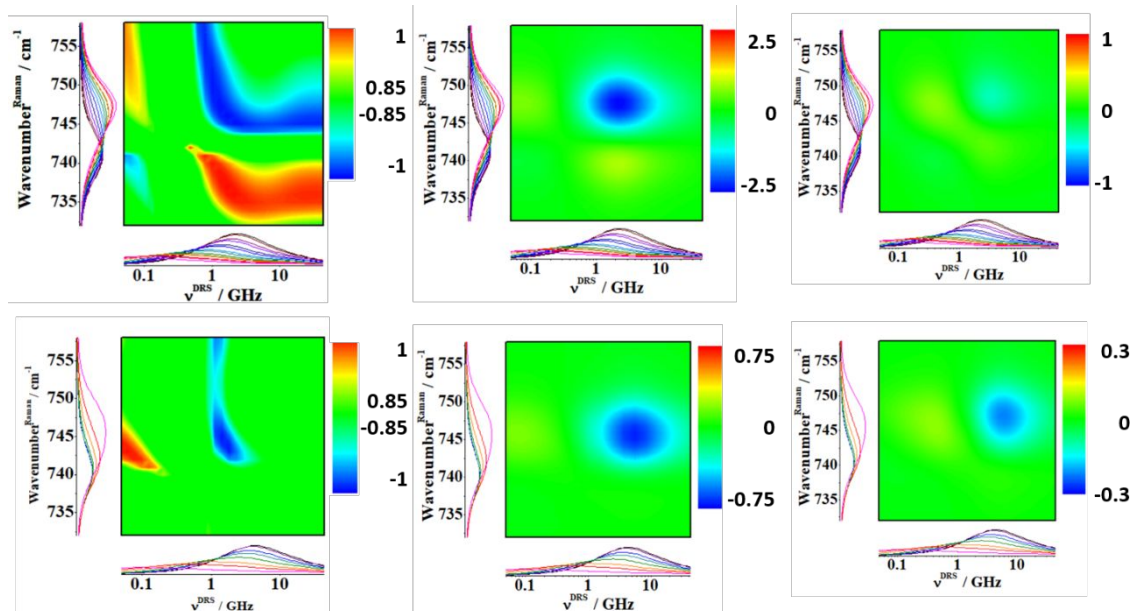


Fig. 6 2D correlation analysis between the Raman spectra of TFSA and the dielectric loss (imaginary part of the complex permittivity). Figure representation is the same as Fig. 5.

spectral intensities increasing or decreasing in the same or opposite direction, similar to Pearson's correlation coefficient. Asynchronous correlations are significant when the apparent Raman intensity at a given wavenumber and the dielectric loss intensity at a given frequency increase or decrease with increasing lithium salt concentration, respectively, and when there is a divergence between these changes.

As clearly indicated in Pearson's correlation coefficients and the Noda-Ozaki synchronous correlation drawn in Fig. 5 and 6, the relaxation of the highest frequency can

be attributed to the free solvent for both PS and SL systems. With regard to the free solvent, the effective dipole moment can be successfully evaluated to be 8.5 and 6.0 for

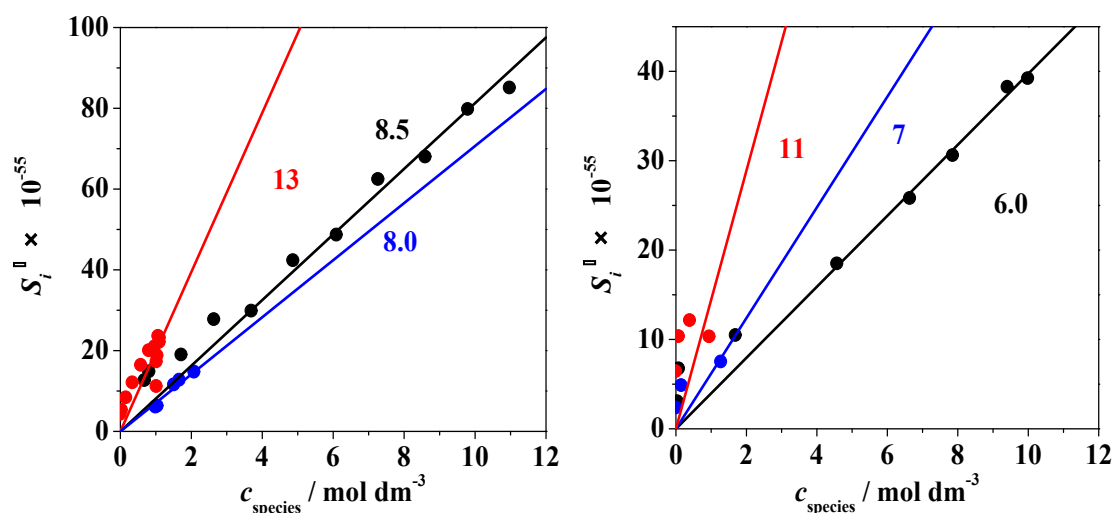


Fig. 7 Relaxation strength vs. the respective polar species concentration determined with the CLSA. S_2^* vs. $c_{f_solvent}$, S_3^* vs. c_{b1_TFSA} and S_4^* vs. c_{b2_TFSA} , are shown in black, red and blue, respectively. Left and right panels are for LiTFSA-PS and LiTFSA-SL systems, respectively.

PS and SL, respectively as shown in Fig. 7, which are consisted with theoretical values in the isolated gas phase. Additionally, the relaxation of the lowest frequency also ascribed to the AGG. Though the assignment is clear in the 2D correlation, it is difficult to estimate accurate and precise the effective dipole moment for the AGG due to the lack of observed frequency and concentration ranges for PS and SL systems, respectively. However, it is worth noting the obtained values are rather small of 8.0 and 7 for PS and SL systems, respectively, as shown in Fig. 7. Such a small dipole moment for the AGG is discussed later. On the other hand, the assignment is unclear for the relaxation of the intermediate frequency. Therefore, we attempted to assess the 2D correlation between the respective calculated spectra to obtain good correlation between the anion bound1 in Raman and the intermediate relaxation in DRS as shown in Fig. S13. However, it should be noted that the synchronous and the asynchronous in the Noda-Ozaki 2D hetero-correlation spectroscopy are considerably small values and remarkably significant relative to those shown in Fig. 5, respectively, so that it is difficult to attribute the relaxation of the intermediate frequency to Raman visible species. However, it is worth evaluating the effective dipole moment based on the anion bound1 concentration, though the estimated effective dipole moment is less accurate and with a large uncertainty than

the free solvent to be 13 and 11 for PS and SL as shown in Fig. 7. This implies that the intermediate relaxation observed in the DRS should consist of several polar species; the solvated solvent molecules, the CIP and probably small size AGGs. Moreover, we should emphasize that the silent in Raman spectrum like the solvent separated/shared ion-pair could yield the dipole response in DRS, and on the contrary the ion-pairs with symmetric charges like a double dimer should be silent in DRS though it involves in both solvent and anion Raman bands as bound species.

Finally, we discuss a time scale of the dipole reorientation observed in DRS. Fig. S14 exhibits the relationship between the solution viscosity η and the relaxation time determined by DRS. All of the indexes evaluated from $\log\eta$ vs. $\log\tau$ were significantly greater than unity, which indicates that the Stokes-Einstein-Debye relationship breaks down for the electrolyte solutions, as easily expected by taking account that the Stokes-Einstein relationship breaks down for the electrolyte solutions. However, it worth mentioning that the relaxation times for the AGG in both mixtures rather slow. As aforementioned, with regard to the glyme based solvent ionic liquids, the extremely slow relaxation was found and they relate with the specific Li^+ conduction in which Li^+ is transported with the solvent/anion exchange. [8] The relaxation time for the AGG in PS and SL systems is also significantly slow, which suggests that the space scale of the AGG should be large. In addition, the estimated effective dipole moments for the AGG in PS and SL systems are rather small, though with less accuracy and large uncertainty, which could be comes from the formation of the large space scale AGG with symmetric charges. However, taking into consideration the fact that Li^+ can be transport much efficiently with the AGG formation in PS and SL systems, we should make much more effort to clarify such an extremely slow relaxation found in new class of liquid electrolyte.

Conclusion

LiTFSA-PS and LiTFSA-SL binary mixture systems were studied by means of DSC, Raman spectroscopy and DRS techniques and DFT calculations. Only the glass transition was observed in the range of $0.1 < x_{\text{Li}} < 0.8$ for PS and $0.1 < x_{\text{Li}} < 0.4$ for SL, which is evidenced these ionic fluids should be a liquid at wide range of lithium composition and temperature. Hence, we believe this class of ionic fluids should be called *glass-forming liquid electrolyte*. Mean solvation numbers and mean anion binding numbers were evaluated for these binary mixtures, which suggests that free, CIP/AGG and AGG species of both the solvent and the anion exist in these binary mixtures. Furthermore, dipole reorientation dynamics for the bulk solvent and the AGG was elucidated, particularly it is implied that the AGG, in which the charges are symmetric to yield relatively a small

dipole moment, has a large space scale. The AGG could play a key role for the unique Li^+ conduction in PS and SL based glass-forming liquid electrolytes.

Author Contributions

Y.U.: supervision and conceptualization of the research, writing a draft and final manuscript. E.O: measurement and analysis of Raman spectra and dielectric relaxation spectra. H.W., J.H.: conceptualization and discussion of the results.

Conflicts of interest

There are no conflicts to declare.

Acknowledgements

The authors express their deep thanks to Prof. Shiro Seki (Department of Environmental Chemistry and Chemical Engineering, School of Advanced Engineering) for technical assistance of the diffusion coefficients by using NMR and Prof. Shigeaki Morita (Department of Engineering Science, Osaka Electro-Communication University) for his valuable discussions. This work was partially supported in part by Grant-in-Aid for Scientific Research (No. 18H01994, 18H03926, 20H05663) from the Japan Society for the Promotion of Science (JSPS) and Ministry of Education, Culture, Sports, Science and Technology (MEXT), Research Fellowships (No. 17J02361 and 20J14822) from the JSPS and the Japan Science and Technology Agency Advanced Low Carbon Technology Research and Development Program Specially Promoted Research for Innovative Next Generation Batteries (JST ALCA-SPRING) Grant Number JPMJAL1301, Japan.

Notes and references

The details of the experimental, data analysis, Raman and DRS spectra, 2D correlation analysis between the Raman spectra and the dielectric loss are described in supporting information.

1. Y. Yamada, K. Furukawa, K. Sodeyama, K. Kikuchi, M. Yaegashi, Y. Tateyama and A. Yamada, *J. Am. Chem. Soc.* 2014, **136**, 13, 5039–5046.
2. Y. Yamada and A. Yamada, *J. Electrochem. Soc.* 2015, **162**, A2406.
3. K. Yoshida, M. Tsuchiya, N. Tachikawa, K. Dokko, and M. Watanabe, MRS Online Proceedings Library 2012, **1473**, 20–25.
4. K. Ueno, K. Yoshida, M. Tsuchiya, N. Tachikawa, K. Dokko and M. Watanabe, *J. Phys. Chem. B* 2012, **116(36)**, 11323–11331.

5. M. Watanabe, K. Dokko, K. Ueno and M.L. Thomas, *Bull.Chem.Soc.Jpn.* 2018, **91**, 1660–1682.
6. D. J. Eyckens and L.C. Henderson, *Front.Chem.* 2019, **7**, 263.
7. A. P. Abbott, G. Capper, D. L. Davies, R. K. Rasheed and V. Tambyrajah, *Chem. Commun.*, 2003, 70-71.
8. C.A. Angell, *J. Electrochem. Soc.* 1965, **112** 1224.
9. C.A. Angell and D.M. Gruen, *J. Am. Chem. Soc.* 1966, **88**, 22, 5192–5198.
10. Y. Yamada, K. Usui, K. Sodeyama, S.J. Ko, Y. Tateyama and A. Yamada, *Nature Energy* 2016, **1**, 16129.
11. N. Arai, H. Watanabe, E. Nozaki, S. Seki, S. Tsuzuki, K. Ueno, K. Dokko, M. Watanabe, Y. Kameda and Y. Umeybayashi, *J. Phys. Chem. Lett.* 2020, **11**, 11, 4517–4523.
12. A. Angell, N. Byrne and J.P. Belieres, *Acc. Chem. Res.* 2007, **40**, 11, 1228–1236.
13. R. Buchner, in *Novel Approaches to the Structure and Dynamics of Liquids: Experiments, Theories and Simulations*, eds. J. Samios and V. A. Durov, NATO Science Series, 2004, pp 265–288.
14. H. Watanabe, T. Umecky, N. Arai, A. Nazet, T. Takamuku, K. R. Harris, Y. Kameda, R. Buchner and Y. Umeybayashi, *J. Phys. Chem. B* 2019, **123**, 29, 6244–6252.
15. N. Arai, H. Watanabe, T. Yamaguchi, S. Seki, K. Ueno, K. Dokko, M. Watanabe, Y. Kameda, R. Buchner and Y. Umeybayashi, *J. Phys. Chem. C* 2019, **123**, 50, 30228–30233.
16. K. Dokko, D. Watanabe, Y. Ugata, M. L. Thomas, S. Tsuzuki, W. Shinoda, K. Hashimoto, K. Ueno, Y. Umeybayashi and M. Watanabe, *J. Phys. Chem. B* 2018, **122**, 47, 10736–10745.
17. A. Nakanishi, K. Ueno, D. Watanabe, Y. Ugata, Y. Matsumae, J. Liu, M. L. Thomas, K. Dokko and M. Watanabe, *J. Phys. Chem. C* 2019, **123**, 23, 14229–14238.
18. J. S. Wilkes, *Geen Chemistry* **2002**, 4 (2), 73–80.
19. T. Welton, *Chem. Rev.* **1999**, 99 (8), 2071–2084.
20. D. MacFarlane, M. Kar and J. M. Pringl, *Fundamentals of ionic liquids : from chemistry to applications*. Weinheim, Germany: Wiley-VCH., **2017**.
21. M. Freemantle, *An Introduction to Ionic Liquids*, Royal Society of Chemistry, **2009**.
22. C. A. Angell, Y. Ansari and Z. Zhao, *Faraday Discuss.* **2012**, 154, 9–27.
23. F. Guthrie, *The London, Edinburgh, and Dublin Philosophical Magazine and Journal of Science*, 5th series., **1884**, 17 (108): 462–482.
24. H. M. A. Abood, A. P. Abbott, A. D. Ballantyne and K. S. Ryder, *Chem. Commun.*, 2011, **47**, 3523–3525.

25. M. Li, B. Gao, C. Liu, W. Chena, Z. Shi, X. Hu and Z. Wang, *Electrochimica Acta* 2015, **180**, 811–814.
26. A. P. Abbott, R. C. Harris, Y.-T. Hsieh, K. S. Rydera and I-W. Sunb, *Phys. Chem. Chem. Phys.* 2014, **16**, 14675.
27. V. S. CVETKOVIĆ¹, N. M. VUKIĆEVIĆ, N. JOVIĆEVIĆ, J. S. STEVANOVIĆ and J. N. JOVIĆEVIĆ, *Trans. Nonferrous Met. Soc. China* 2020, **30**, 823–834.
28. J. S. Wilkes, J. A. Levisky, R. A. Wilson and C. L. Hussey, *Inorganic Chemistry*, 1982, **21**, 3.
29. J. S. Wilkes, J. A. Levisky, J. L. Pflug, C. L. Hussey and T. B. Scheffler, *Anal. Chem.* 1982, **54**, 13, 2378–2379.
30. A. A. Fannin, Jr., D. A. Floreani, L. A. King, J. S. Landers, B. J. Piersma, D. J. Stech, R. L. Vaughn, J. S. Wilkes and J. L. Williams, *J. Phys. Chem.* 1984, **88**, 2614–2621.
31. M. Esteban, C. Ariño, J. M. Díaz-Cruz, M. S. Díaz-Cruz and R. Tauler, *Trends Anal. Chem.* 2000, **19**, 49–61.
32. J. Jaumot, R. Gargallo, A. de Juan and R. Tauler, *Intell. Lab. Syst.* 2005, **76**, 101–110.
33. S. Hwang, D.-H. Kim, J. H. Shin, J. E. Jang, K. H. Ahn, C. Lee, and H. Lee, *J. Phys. Chem. C* 2018, **122**, 34, 19438–19446.
34. H. Lee, S. Hwang, M. Kim, K. Kwak, J. Lee, Y.-K. Han, and H. Lee. *J. Phys. Chem. Lett.* 2020, **11**, 24, 10382–10387.
35. J. Self, N. T. Hahn, K. D. Fong, S. A. McClary, K. R. Zavadil and K. A. Persson, *J. Phys. Chem. Lett.* 2020, **11**, 6, 2046–2052.
36. J. Kim, B. Koo, J. Lim, J. Jeon, C. Lim, H. Lee, K. Kwak and M. Cho, *ACS Energy Lett.* 2022, **7**, 1, 189–196.
37. B. Koo, H. Lee, S. Hwang and H. Lee, *J. Phys. Chem. C*, 2023, **127**, 12, 5676–5682.
38. B. Koo, H. Lee, S. Hwang, J. Lee, Y.-K. Han, K. Ahn, C. Lee and H. Lee, *J. Phys. Chem. C* 2023, **127**, 18271–18278.
39. J. Self, N. T. Hahn, K. A. Persson, *Energy Environ. Mater.* 2024, **7**, e12494.
40. E.A.S. Cavell, P.C. Knight, M. A. Sheikh, *Trans. Faraday Soc.* 1971, **67**, 2225–2233.
41. J. Barthel, H. Hetzenauer, R. Buchner, *Berichte der Bunsengesellschaft für physikalische Chemie* 1992, **96**, 10, 1424–1432.
42. K. Pearson, F.R.S. and A. LEE, D.Sc, *Biometrika*, 1903, **2**, 4, 357–462.
43. I. Noda and Y. Ozaki, *Two-Dimensional Correlation Spectroscopy*, John Wiley & Sons, 2005.
44. Y. Ozaki, S. Šašić, T. Tanaka and I. Noda, *Bull. Chem. Soc. Jpn.* 2001, **74**, 1–17.